LES of atomizing spray with stochastic modeling of secondary breakup

S.V. Apte [a,*], M. Gorokhovski [b,1], P. Moin [c]

[a] *Department of Mechanical Engineering, Stanford University, Bldg. 500, ME/FPC, 488 Escondido Mall, Stanford, CA 94305-3030, USA*
[b] *Department of Energetics, IUT, University of Rouen, FR-76821, Mont Saint Aignant, France*
[c] *CTR, Stanford University, Bldg. 500, ME/FPC Stanford, CA 94305-3030, USA*

Abstract

A stochastic subgrid model for large-eddy simulation of atomizing spray is developed. Following Kolmogorov's concept of viewing solid particle-breakup as a discrete random process, atomization of liquid blobs at high relative liquid-to-gas velocity is considered in the framework of uncorrelated breakup events, independent of the initial droplet size. Kolmogorov's discrete model of breakup is rewritten in the form of differential Fokker–Planck equation for the PDF of droplet radii. Along with the Lagrangian tracking of spray dynamics, the size and number density of the newly produced droplets is governed by the evolution of this PDF in the space of droplet-radius. The parameters of the model are obtained dynamically by relating them to the local Weber number with two-way coupling between the gas and liquid phases. Computations of spray are performed for the representative conditions encountered in idealized diesel and gas-turbine engine configurations. A broad spectrum of droplet sizes is obtained at each location with co-existence of large and small droplets. A novel numerical algorithm capable of simultaneously simulating individual droplets as well as a group of droplets with similar properties commonly known as parcels is proposed and compared with standard parcels-approach usually employed in the computations of multi-phase flows. The present approach is shown to be computationally efficient and captures the complex fragmentary process of liquid atomization.
© 2003 Elsevier Ltd. All rights reserved.

Keywords: LES; Sprays; Atomization & breakup; Particle-laden flows; Stochastic modeling; Unstructured grid; Complex combustors

---

[*] Corresponding author. Tel.: +1-650-725-1821; fax: +1-650-725-3525.
E-mail address: sapte@stanford.edu (S.V. Apte).
[1] Visiting fellow, CTR, Stanford University, Stanford, CA, USA.

1. Introduction

Liquid spray atomization plays a crucial role in analyzing the combustion dynamics in many propulsion related applications. This has led researchers to focus on modeling of droplet formation in numerical investigations of chemically reacting flows with sprays. In the traditional approach for spray computation, the Eulerian equations for gaseous phase are solved along with a Lagrangian model for particle transport with two-way coupling of mass, momentum, and energy exchange between the two phases (Dukowicz, 1980). The spray atomization process is modeled by standard deterministic breakup models based on Taylor analogy breakup (TAB) (O'Rourke and Amsden, 1987) or wave (Reitz, 1987) models. Liquid 'blobs' with the size of the injector diameter are introduced into the combustion chamber and undergo atomization based on the balance between aerodynamic and surface tension forces acting on the liquid phase.

In the TAB model (O'Rourke and Amsden, 1987), oscillations of the parent droplet are modeled in the framework of a spring mass system and breakup occurs when the oscillations exceed a critical value. In the wave model, new droplets are formed based on the growth rate of the fastest wave instability on the surface of the parent blob (Reitz, 1987). Both models are deterministic with 'single-scale' production of new droplets. In many combustion applications, however, injection of liquid jet takes place at high relative velocity between the two phases (high initial Weber number). Under these conditions, intriguing processes such as turbulence-induced breakup (Chigier and Reitz, 1996), multiple droplet collision in the dense spray region (Georjion and Reitz, 1999), fluctuations due to cavitating flow inside the injector (Lefebvre, 1989), etc., contribute to the process of atomization. At each spray location, this may result in droplet formation over a large spectrum of droplet-sizes and is not captured by the above models. In order to improve the TAB model, Tanner (1998) used an enhanced TAB model (ETAB), where the product droplet size was obtained via a breakup cascade modeled by an exponential law. The parameters of this distribution function were derived from experimental data to achieve better performance of the model.

To predict the essential global features of these complex phenomena, a stochastic approach for droplet breakup taking into account a range of product-droplet sizes is imperative (Gorokhovski, 2001). In the present work, we develop such an approach coupled with large-eddy simulation (LES) of the gas-phase. Specifically, at a given control volume, the characteristic radius of droplets is assumed to be a time-dependent stochastic variable with a given initial distribution function. The breakup of parent blobs into secondary droplets is viewed as the temporal evolution of this distribution function. The size of new droplets can be sampled from the distribution function evaluated at a typical breakup time scale of the parent drop. Owing to the complexity of the phenomenon, it is difficult to clearly identify a dominant mechanism for breakup and the corresponding behavior of the distribution function. On the other hand, for a series of uncorrelated breakup events, Kolmogorov (1941) developed a stochastic theory where the breakup of solid particles is modeled by a discrete random process. The probability to break each parent particle into a certain number of parts is assumed independent of the parent-particle size. Using central limit theorem, Kolmogorov pointed out that such a general assumption leads to a lognormal distribution of particle size in the long-time limit. Further theoretical developments of Kolmogorov's stochastic theory can be found in Gorokhovski and Saveliev (2003).

In this work, we develop a numerical scheme for atomization of liquid spray at large Weber number based on Kolmogorov's hypothesis. The discrete model by Kolmogorov is reformulated in terms of a Fokker–Planck (FP) differential equation for the evolution of the size-distribution function from a parent-blob towards the log-normal law. The secondary droplets are sampled from its analytical solution corresponding to the breakup time scale. The parameters encountered in the FP equation are computed dynamically by relating them to the local Weber number. The capillary force prescribes a lower bound for the produced-droplet size through the local maximum stable (or critical) radius. The velocity of the produced droplets is modeled using Monte Carlo procedure and Lagrangian tracking in the physical space is continued till further breakup events. The evolution of droplet diameter is basically governed by the local scale of relative-velocity fluctuations between the gas and liquid phases. In this respect, LES plays a key role in providing accurate, local estimates of the gas-phase turbulent quantities (Moin and Kim, 1987). Although the mesh spacing used in a typical LES computation is larger than droplet size, the superiority of LES over RANS lies in accurate predictions of mixing and momentum transport from the gas phase to the spray field.

Furthermore, the standard approach of representing a group of like-droplets called 'parcels' (computational particles) is inappropriate in the context of LES. Computational parcels provide averaged particle properties as opposed to instantaneous ones required in LES. Theoretically, all droplet trajectories should be computed to accurately represent the coupling between the gas and liquid phases. This, however, leads to unacceptably large number of computational particles within a short period of time, making it impossible to simulate even with advanced parallel computing techniques. A novel hybrid-approach involving co-existence of individual droplets and parcels (computational particle) is developed. Tracking of parcels and droplets is shown to be an efficient way of performing spray simulations. The superiority of the hybrid-approach along with the present stochastic model in predicting atomization and spray-evolution is demonstrated by comparing the instantaneous snapshots of spray with those obtained by standard parcels-approach. Finally, the importance of the present model for the computation of high-speed air-blast atomization encountered in gas-turbine combustion chambers is demonstrated by computing the breakup of round water jet in a turbulent channel flow. The spatial distribution of droplets indicating a turbulent, flapping spray with large unbroken drops in the near-injector region and temporal evolution of bursting droplets in the far-field is demonstrated. The interaction between turbulence and atomization is explored by computing one-point correlations between the gas-phase streamwise velocity component and droplet size.

In subsequent sections, Kolmogorov's stochastic theory of solid particle breakup is summarized. The discrete breakup model is applied to atomization by constructing a Fokker–Planck equation and obtaining the long-time analytical solutions. Next, a numerical algorithm implementing the present model into a Eulerian–Lagrangian solver along with the hybrid-technique for spray computations is described. Results obtained from a series of numerical simulations in idealized diesel and gas-turbine configurations are presented.

2. Fokker–Planck equation for particle-breakup

Let $N_{\text{tot}}(t)$ and $N(r,t)$ represent the total number of breaking particles and particles with size $\rho \leqslant r$, respectively, at discrete time instants $t = 0, 1, 2, \ldots$ These time moments are scaled by the

breakup frequency, v, such that ($v t_{bu} = 1$), where t_{bu} is the time at which breakup occurs. Their corresponding expectations are given as $\overline{N}_{tot}(t)$ and $\overline{N}(r,t)$, respectively. Consider breakup of a given particle with size r within the time interval $[t, t+1]$. Let $Q(\alpha)$ be the mean number of secondary particles produced with size $\rho \leqslant \alpha r$, with $0 \leqslant \alpha \leqslant 1$. According to Kolmogorov's hypothesis, the probability to break each parent particle into a given number of fragments is independent of the parent particle size. In other words, $Q(\alpha)$ does not depend on the history of breakup and is not influenced by other parent particles. It then follows that

$$\overline{N}(r, t+1) = \int_0^1 \overline{N}(r/\alpha, t)\, \mathrm{d}Q(\alpha) \tag{1}$$

Introducing $x = \ln(r)$, Kolmogorov pointed out that

$$T(x, t) = \frac{\overline{N}(e^x, t)}{\overline{N}_{tot}(t)} = \frac{N(e^x, t)}{N_{tot}(t)} \tag{2}$$

Further, denoting $\xi = \ln(\alpha)$ and $Q(\alpha) = Q(1) \cdot S(\xi)$, Eq. (1) can be rewritten as

$$T(x, t+1) = \int_{-\infty}^0 T(x - \xi, t)\, \mathrm{d}S(\xi) \tag{3}$$

By central limit theorem, Kolmogorov noted that from discrete model (Eq. (3)), the long-time limit form of $T(x,t)$ approaches an error function (Eq. (12) from Kolmogorov, 1941). This implies that the number of droplets $N(r,t)$ is asymptotically governed by the log-normal density distribution of particle size. The entire spectrum, $Q(\alpha)$, is unknown. However, in the limit of large time Eq. (3) can be represented by Fokker–Planck differential equation where only the first two moments of $Q(\alpha)$ are considered important. Using parabolic scaling of variables, $\tau = \beta^2 t$, $y = \beta x$, where β is a scaling parameter ($\beta \to 0$ as $t \to \infty$) and t is scaled by the breakup frequency v, Eq. (3) can be written as

$$T(y, \tau + \beta^2) = \int_{-\infty}^0 T(y - \beta\xi, \tau) S(\xi)\, \mathrm{d}\xi \tag{4}$$

Expanding both the left-hand side and the expression under integral in Eq. (4), with the assumption that $\int_{-\infty}^0 \xi^3 S(\xi)\, \mathrm{d}\xi$ is limited such that $\frac{1}{6}\beta \frac{\partial^3 T}{\partial x^3} \int_{-\infty}^0 \xi^3 S(\xi)\, \mathrm{d}\xi$ becomes negligible if $\beta \to 0$, one obtains the Fokker–Planck approximation:

$$\frac{\partial T(x,t)}{\partial t} = -v\langle\xi\rangle \frac{\partial T(x,t)}{\partial x} + \frac{1}{2}v\langle\xi^2\rangle \frac{\partial^2 T(x,t)}{\partial x^2} \tag{5}$$

where $\langle\xi\rangle = \int_{-\infty}^0 \xi S(\xi)\, \mathrm{d}\xi$ and $\langle\xi^2\rangle = \int_{-\infty}^0 \xi^2 S(\xi)\, \mathrm{d}\xi$ are the first two moments of ξ. Eq. (5) can be rewritten for the probability density distribution, $\Phi(x)$ by substituting $T(x,t) = \int_{-\infty}^x \Phi(x,t)\, \mathrm{d}x$,

$$\frac{\partial \Phi(x,t)}{\partial t} + v\langle\xi\rangle \frac{\partial \Phi(x,t)}{\partial x} = \frac{1}{2}v\langle\xi^2\rangle \frac{\partial^2 \Phi(x,t)}{\partial x^2} \tag{6}$$

The number distribution of radius, $f(r,t)$, normalized on the total number of particles $\int_0^\infty f(r,t)\, \mathrm{d}r = 1$, can be expressed according to the rule, $|f(r)\, \mathrm{d}r| = |\Phi(x)\, \mathrm{d}x|$. This gives

$$\Phi(x) = e^x f(e^x); \qquad f(r) = \frac{1}{r}\Phi(\ln r) \tag{7}$$

Using Eq. (7), the Fokker–Planck equation for the distribution $f(r,t)$ is

$$\frac{\partial f(r,t)}{\partial t} = \frac{\partial S(r,t)}{\partial r} \tag{8}$$

where $S(r,t)$ is the flux density in the space of length scales given by the following expression:

$$S(r,t) = -v\langle\xi\rangle r f(r,t) + \frac{1}{2}v\langle\xi^2\rangle r \frac{\partial}{\partial r}(rf(r,t)) \tag{9}$$

The solution of Eq. (6) is a Gaussian function given by

$$\Phi(x,t) = \int_{-\infty}^{0} \frac{1}{\sqrt{2\pi\langle\xi^2\rangle vt}} \exp\left[\frac{-(x-x_0)^2}{2\langle\xi^2\rangle vt}\right] \Phi_0(x_0 - \langle\xi\rangle vt)\,\mathrm{d}x_0 \tag{10}$$

where $\Phi_0(x_0)$ is the initial distribution of the logarithm of droplet radius and x_0 is logarithm of radius of the parent drop. Accounting for Eq. (7), this solution can be rewritten for the normalized distribution of radius, $f(r,t)$:

$$f(r,t) = \frac{1}{r}\int_{0}^{\infty} \frac{1}{\sqrt{2\pi\langle\xi^2\rangle vt}} \exp\left[\frac{-(\log(r_0/r) + \langle\xi\rangle vt)^2}{2\langle\xi^2\rangle vt}\right] f_0(r_0)\,\mathrm{d}r_0 \tag{11}$$

where $f_0(r_0)$ is the initial distribution of droplet radius before breakup.

3. Implementation of stochastic breakup model into unstructured LES code

In the present LES computations, an Eulerian–Lagrangian code based on low Mach number equations is used (Mahesh et al., submitted). This code is capable of handling complex geometries with unstructured and arbitrary shaped elements and is primarily developed for hi-fidelity computations of turbulent flows in realistic combustors. This algorithm has been validated for multiphase flows in a variety of configurations including turbulent flows through channel, swirling coaxial combustor, and realistic industrial combustion chamber (Mahesh et al., 2001; Apte et al., 2003).

The influence of the high number density of droplets on the gas-phase flow are modeled through two-way coupling between the gas and liquid phase. The standard particle-in-cell methodology is employed where the effect of particles within a control volume is represented at its centroid. The Lagrangian equations governing the particle motions are

$$\frac{\mathrm{d}\mathbf{x}_p}{\mathrm{d}t} = \mathbf{u}_p \tag{12}$$

$$\frac{\mathrm{d}\mathbf{u}_p}{\mathrm{d}t} = \frac{f}{St_p}(\mathbf{u} - \mathbf{u}_p) \tag{13}$$

where $\mathbf{x}_p$, $\mathbf{u}_p$, $\mathbf{u}$ are the droplet position, velocity, and gas-phase velocity vectors, respectively. f is the drag coefficient and St_p, the particle Stokes number defined as

$$St_{p} = \frac{1}{18}\rho_{p}d_{p}^{2}Re_{ref} \tag{14}$$

where $Re_{ref} = \rho_{ref}U_{ref}L_{ref}/\mu_{ref}$ is based on the reference length and velocity scales used to normalize the governing equations. The drag coefficient f has several expressions as a function of particle Reynolds number, $Re_{p} = d_{p}Re_{ref}|\mathbf{u} - \mathbf{u}_{p}|$. For particle Reynolds number up to 800, Schiller and Naumann (see Crowe et al., 1998) proposed a nonlinear correlation:

$$f = (1 + aRe_{p}^{b}) \tag{15}$$

This yields a drag coefficient with less than 5% deviation from the standard drag curve for $a = 0.15$, $b = 0.687$. The gas-phase velocity, $\mathbf{u}$, in Eqs. (12) and (13) are computed at individual particle locations within a control volume using a generalized, tri-linear interpolation scheme for arbitrary shaped elements. More details of this formulation are given in Apte et al. (2003).

The present paper focuses on the details of the secondary atomization model and efficient computation of spray breakup. First, the implementation of the stochastic breakup model into the unstructured LES code is described in detail. Later, the hybrid-algorithm and its implementation are explained.

3.1. Procedure for computation of breakup

The liquid-sheet injected into the computational domain is represented by large 'blobs' with characteristic size equal to the injector nozzle radius and a given velocity. These large drops are tracked with two-way coupling between the gas and liquid phases. The breakup model then predicts the time at which these blobs would break as well as the number and properties of the formed droplets based on a Monte Carlo procedure. Specifically, the product droplet velocity and the local magnitude of the critical (or maximum stable) radius, r_{cr}, are obtained. Newly formed droplets replace the present one in the statistical representation of spray.

Consider motion of a jth primary drop that undergoes breakup ($r_{j} > r_{cr}$). As new drops/blobs are formed/introduced into the domain, the size-distribution function associated with them is a Dirac-delta function. Initially, their age, t, is presumed to be zero and increases as they evolve along with the flowfield. With $t \geqslant t_{bu} \equiv 1/v$ and $We_{j} > We_{cr}$, new droplets are created based on the droplet-radius distribution function, which evolves according to Eq. (10). The number and size of these droplets is determined based on the stochastic sampling procedure and by conserving mass of the parent drop. The parent drops/blobs are destroyed and Lagrangian tracking of newly formed droplets is continued till the next breakup event ($vt = 1, r_{j} > r_{cr}$). In the present computations, we used expressions obtained for the distribution of the logarithm of radius. The initial distribution for the logarithm of radius of the jth primary drop can be represented as

$$\Phi_{0j}(x_{0}) = \delta(x_{0} - x_{j}) \tag{16}$$

Using the distribution function from Eq. (10), the solution can be expressed as

$$T_{j}(x, t+1) = \int_{-\infty}^{x} \Phi_{j}(x, t)\,\mathrm{d}x = \frac{1}{2}\left[1 + erf\left(\frac{x - x_{j} - \langle\xi\rangle}{\sqrt{2\langle\xi^{2}\rangle}}\right)\right] \tag{17}$$

The product droplet velocity is computed by adding a factor $\mathbf{w}_{bu}$ to the primary drop velocity. This additional velocity is randomly distributed in a plane normal to the relative velocity vector between the gas-phase and parent drop, and the magnitude is determined by the radius of the parent drop and the breakup frequency, v:

$$|\mathbf{w}_{bu}| = rv \tag{18}$$

This modification of newly formed droplets follows the physical picture of parent droplets being torn apart by aerodynamic forces giving momentum to the newly formed droplets in the direction normal to the relative velocity between the gas-phase and parent drops (O'Rourke and Amsden, 1987).

3.2. Critical radius and breakup frequency

The critical (or maximum stable) radius for breakup is obtained by a balance between the disruptive hydrodynamic and capillary forces:

$$r_{cr} = \frac{We_{cr}\sigma}{\rho_g u_{r,j}^2} \tag{19}$$

where $|u_{r,j}|$ is the relative velocity between the gas and droplet, σ the surface tension coefficient, We_{cr} the critical Weber number, which is assumed to be of the order of six over a wide range of Ohnesorge numbers (Gel'fand et al., 1975; Pilch and Erdman, 1987). For highly turbulent flows, however, the instantaneous value of Kolmogorov's scale, η, is often less than the droplet size and the entire spectrum of turbulent kinetic energy can contribute to the stretching and disintegration of the droplet. In this case, the critical radius should be obtained as a balance between the capillary forces and turbulent kinetic energy supplied to the liquid droplet. Kolmogorov (1949) defined a critical droplet radius through an equivalent relative velocity based on his theory of local statistical properties in high Reynolds number,

$$u_{r,j}^2 = \left(\frac{v_{lam}}{\eta}\right)^2 \left(\frac{d}{\eta}\right)^{2/3} \tag{20}$$

where d is the droplet diameter. Similar expression was used by Martinez-Bazan et al. (1999) to obtain frequency of bubble breakup in turbulent flows. Eq. (20), however, does not account for the liquid density, while inertia effects play an important role in droplet stretching. Accordingly, this expression can be further modified by estimating the r.m.s. of relative droplet-to-gas velocity from the mean viscous dissipation and Stokes time scale (Kuznezov and Sabel'nikov, 1990):

$$\langle u_{r,j}^2 \rangle \approx \epsilon\tau_{st} \tag{21}$$

Using Eqs. (19) and (21), one obtains

$$r_{cr} = \left(\frac{9}{2} \frac{We_{cr}\sigma v_{lam}}{\epsilon\rho_l}\right)^{1/3} \tag{22}$$

This expression, however, requires a reliable knowledge of viscous dissipation rate and can be easily obtained dynamically from the resolved scale energy flux in a LES computation. The

breakup frequency is obtained following the analogy with expressions used for aerodynamic breakup and utilizing the relative velocity, $|u_{r,j}|$, given by Eq. (21)

$$t_{\text{bu}} = B \frac{\sqrt{\rho_l}}{\rho_g} \frac{r_j}{|u_{r,j}|} \tag{23}$$

where r_j is the radius of parent drop and $B = \sqrt{1/3}$ (O'Rourke, 1981; Faeth et al., 1995).

3.3. Choice of parameters $\langle \xi \rangle$ and $\langle \xi^2 \rangle$

Multiplying Eq. (9) by r and integrating over the entire range gives an expression for the first moment

$$\langle r \rangle = \langle r \rangle_{t=0} \exp[v(\langle \xi \rangle + 0.5\langle \xi^2 \rangle)t] \tag{24}$$

Further more, the expression

$$\langle \xi \rangle + \frac{1}{2}\langle \xi^2 \rangle < 0 \tag{25}$$

is a necessary condition to obtain disintegration of parent droplets, $\frac{\langle r \rangle}{\langle r \rangle_{t=0}} < 0$. Providing values of $\langle \xi \rangle$ and $\langle \xi^2 \rangle$ is a crucial and difficult problem similar to closure of turbulence models. Our objective is to relate these terms to the characteristic flow parameters in order to obtain their values dynamically. It should be noted that in the long time limit, when all droplets are broken, the flux density in the space of radius $S(r, t \to \infty)$ can be set to zero to provide a steady state distribution of broken droplets. Equating Eq. (9) to zero, one obtains the power law distribution

$$f(r,t)|_{t\to\infty} \sim \left(\frac{1}{r}\right)^{(1-2\langle \xi \rangle/\langle \xi^2 \rangle)} \tag{26}$$

A power distribution is endowed with self-similarity of fractal property of irregular shapes. The fractal structure of atomizing spray was observed by Shavit and Chigier (1995) and Zhou and Yu (2000). This implies that in the intermediate range of scales between the parent fluid element (large Weber number) and the maximum stable droplet (critical Weber number) there exists no preferred length scale. This closely resembles the inertial range of the energy cascade process in homogeneous turbulence at high Reynolds numbers. Analogously, assuming $u_{r,j}^3/r_j \sim u_{r,\text{cr}}^3/r_{\text{cr}}$, one obtains

$$\frac{r_{\text{cr}}}{r_j} \sim \left(\frac{We_{\text{cr}}}{We_j}\right)^{3/5} \Rightarrow \langle \log \alpha \rangle \equiv \langle \xi \rangle = K_1 \log \left(\frac{We_{\text{cr}}}{We_j}\right) \tag{27}$$

where $u_{r,\text{cr}}$ is the relative velocity at which disruptive forces are balanced by capillary forces (similar to turbulent velocity scale of the smallest eddies).

From Einstein's theory of Brownian motion, the diffusion coefficient in the Fokker–Planck equation is known to be the energy of Brownian particles multiplied by their mobility. In the present theory, the drift velocity is presented in the form of drag force times the mobility. The ratio of diffusion to drift velocity is given by the ratio of energy to drag force. In the breakup process, we associate the energy in Einstein's theory with the disruptive energy while the force to the capillary force on the droplet. Their ratio is represented by the maximum stable droplet radius,

r_{cr}. Considering the Fokker–Planck equation (Eq. (8)), the diffusion to drift velocity ratio is scaled by $-\langle \xi^2 \rangle / \langle \xi \rangle$. Then it is assumed that

$$-\frac{\langle \xi \rangle}{\langle \xi^2 \rangle} \equiv -\frac{\langle \log \alpha \rangle}{\langle \log^2 \alpha \rangle} = K_2 \log \left(\frac{r_j}{r_{cr}} \right) \tag{28}$$

were K_1 and K_2 are model constants of order unity. The parameters in the Fokker–Planck equation are obtained dynamically by using Eqs. (27) and (28).

4. Hybrid droplet-parcel algorithm for spray computations

Performing spray breakup computations using Lagrangian tracking of each individual droplet gives rise to a large number of droplets (of the order 50 million) very close to the injector. In parallel computation of complex flows utilizing standard domain-decomposition techniques, the load balancing per processor is achieved by equally distributing the number of grid cells among all processors. Lagrangian particle-tracking causes load-imbalance owing to the varying number of droplets per processor. Dynamic-load balancing and redistribution of the load as the spray evolves is necessary to resolve the load imbalance caused by spray computations. This, however, is difficult to implement in an unstructured code utilizing arbitrary domain decomposition and is an important area of applied mathematics research.

In order to overcome the load-imbalance issue, usually a group of droplets with similar characteristics (diameter, velocity, temperature, etc.) is represented by a computational particle or 'parcel' to decrease the total number of Lagrangian particles tracked in a simulation. Each parcel carries the number of droplets per parcel as a parameter. With breakup, the diameter of the parcel is sampled according to the procedure given above and the number of droplets associated with the particles is changed in order to conserve mass. No additional computational particles are created owing to breakup. This reduces the total number of particles per processor and the computational overhead with sprays is only around 20–30% depending on the number of parcels used. Each parcel has all the droplet characteristics associated with it. The parcels-methodology works well for RANS-type simulations where one is interested in time- or ensemble-averaged quantities. For deterministic breakup models such as the wave and TAB models, same size droplets are created after breakup and grouping of droplets using parcels approach seems reasonable. In the present stochastic model, breakup occurs over a wide range of droplet sizes and the parcels-approach is not appropriate as shown later.

A hybrid scheme involving the computation of both individual droplets and parcels is proposed. The difference between droplets and parcels is simply the number of particles associated with them N_{par}, which is unity for droplets. During injection, new particles introduced in the computational domain are pure drops ($N_{par} = 1$). These drops move downstream and undergo breakup according to the procedure given in Section 2 and produce new droplets thus increasing the number of computational particles in the domain. In the dense-spray regime, one may obtain large number of droplets in a control volume and its immediate neighbors. The basic idea in the hybrid-approach is to group these droplets into bins corresponding to their size and other properties such as velocity, temperature etc. The droplets in bins are then collected to form a parcel by conserving mass, momentum and energy. The location of the parcel is obtained by mass-weighted averaging from

individual drops in the bin. The parcel thus created then undergoes breakup according to the above stochastic sub-grid model, however, does not create new parcels. On the other hand, the number of particles associated with the parcel is increased and the diameter is decreased by mass-conservation.

The collection and grouping of droplets belonging to same control volume can be achieved easily by defining pointer arrays as shown in Fig. 1. First, the number of droplets (it should be noted here that only droplets are considered in this grouping and parcels within the control volume are excluded) present in all control volumes (N_{cv}) on a processor is counted. Creation of parcels from the individual droplets proceeds if the total number of droplets per cell exceeds a prescribed threshold. This criterion helps in restraining the total number of computational particles per processor from growing to unreasonable values. A CV list is then formed which points to the beginning of an array consisting of group of particles termed as droplet-index. The droplet-identifier points to the serial number of each droplet. The total number of droplets in each group of droplet-identifier is obtained from the CV list. This grouping methodology is fast and is achieved by looping twice over the number of control volumes and once over the total number of particles per processor. With this re-grouping technique, the total number of droplets in each cell is readily available. The list of particle numbers in a particular control volume can be accessed by using the droplet serial number and droplet-identifier arrays.

Finally, only those cells (for example, CV = 1 as shown in Fig. 1) are considered for which the number of droplets (DI_1) exceeds a predetermined threshold. These droplets are now distributed into bins. PDFs and droplet number densities are constructed based on the droplet diameter, velocity, and other properties. In the present work the temperature of all droplets is same as the gas-phase and evaporation is negligible. It was observed that droplets distributed into bins based only on their size gave similar results as compared to a two-dimensional sorting based on diameter and realtive velocity. In Fig. 1 five droplet size classes are considered with the minimum and maximum diameters equal to those obtained in CV = 1. The individual droplets are now destroyed
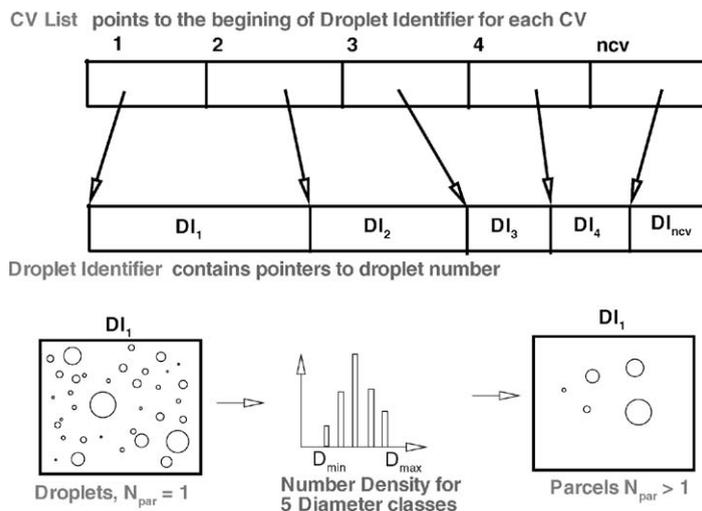

Fig. 1. The hybrid particle/parcel algorithm.

and new parcels are created. It should be noted that, the diameter of the parcels is obtained from the mass-averaging of the individual droplet sizes in a bin. This is different compared to modeling the effect of coalescence. The result of coalescence is one droplet of larger size while the parcel formed represents mass-averaged size of the droplets in the bin. Improvements and standardization of the above methodology can be achieved by monitoring the number density per control volume. In addition, advanced droplet coalescence and collision models (Schmidt and Rutland, 2000) can be easily implemented in this framework.

The effectiveness of this hybrid approach is demonstrated in the following computations. The implementation of this method in an unstructured LES code gives us the capability of testing and validating these models in realistic industrial geometries for various combustors with multiphase flows.

5. Spray evolution in diesel-engine configuration

In order to validate the stochastic breakup model together with the hybrid algorithm proposed herein, a standard test case for spray atomization in a diesel-engine configuration is simulated and compared with the experimental data of Hiroyasu and Kadota (1974). The computational domain is a closed cylinder of length 13.8 cm and diameter 5.6 cm. Liquid jet is injected through a single-hole nozzle into this constant pressure, room-temperature nitrogen chamber. Since the chamber temperature is low, evaporation of the liquid fuel is negligible. Large blobs of diameter 300 μm corresponding to the nozzle size are injected into the combustion chamber. Initially, there is no gas-phase flow inside the chamber. Gas-phase recirculation zones are created through momentum transfer from the liquid jet to the gas-phase. Three cases with different chamber pressures of 1.1, 3, and 5 MPa are simulated in order to validate with the experimental data. The corresponding flow parameters are indicated in Table 1. The mass flow rate of the liquid is obtained from the injection velocity, nozzle diameter and the time of injection. The number of droplets injected per iteration is determined based on the droplet diameter and time step by keeping the mass flow rate constant. The time step used in the present simulation is 15 μs and a uniform grid of $100 \times 65 \times 65$ cells is found to capture the spray dynamics accurately.

Fig. 2 shows the time evolution of the distribution of droplets in the combustion chamber. The region close to the injector mostly consists of large-unbroken drops along with small, stripped droplets. The ligament-like liquid structures deflected outward are clearly visible. Hiroyasu and Kadota (1974) provided an experimental correlation to estimate the intact liquid core length,

Table 1
Validation cases for stochastic breakup model in diesel-engine configuration (Hiroyasu and Kadota, 1974)

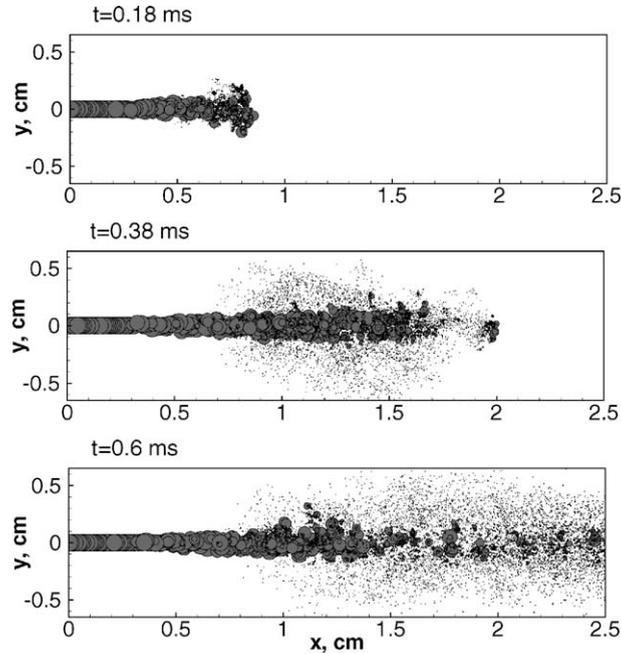| Parameters	Case 1	Case 2	Case 3
P_{liq}, MPa	10	10	10
P_{gas}, MPa	1.1	3.0	5.0
Injection diameter, μm	300	300	300
Injection time, ms	2.5	4.0	5.0
Injection velocity, m/s	102	90.3	86.4

Fig. 2. Time evolution of spray in a nitrogen-filled closed cylindrical chamber at 1.1 MPa using the hybrid approach.

$L = 0.5Ad_0\sqrt{\rho_l/\rho_g}$, where d_0 is the nozzle diameter (300 µm in the present case). Values of A of 14 and 25 yield the minimum and maximum measured lengths, respectively. For the case with chamber pressure of 1.1 MPa, these lengths are 1.5 and 3 cm, respectively. Based on the time evolution of the spray in the present simulations, the minimum intact core length (the maximum distance from nozzle where large unbroken drops are observed) is around 1.2 cm. It should be noted that, initially the gas-phase in the chamber is at rest. With injection of droplets from the nozzle, recirculation zones are created through momentum exchange between the liquid and gas-phase. The relative velocities experienced by the first injected large drops are thus higher and breakup is initiated earlier. With time, however, large unbroken drops were observed till 2.5 cm from the nozzle. Reitz (1987) defines the (partial) core length of spray as

$$L_{d_0/2} = \max(l_j | d_j < d_0/2) \tag{29}$$

where d_j and d_0 are the drop and nozzle diameters, respectively and l_j is the distance from the nozzle exit to the location of jth droplet. Here the maximum is taken over all droplets close to the inejector. Accordingly, $L_{d_0/2}$ is 2.5 cm in the present computation which is close to the values reported by Reitz (1987) and Tanner (1998).

Fig. 3 shows the comparison of the spray-tip penetration depth as a function of time with the experimental data for the three cases investigated. Good agreement is obtained for all the three cases with the model parameters obtained dynamically from the local flow conditions. The penetration depth decreases with increase in pressure as seen from Fig. 3. This is attributed to the decreased injection velocity as well as strong damping of the liquid momentum by the denser gas-phase at higher pressures. Fig. 4 shows the probability density function of mass distribution in the
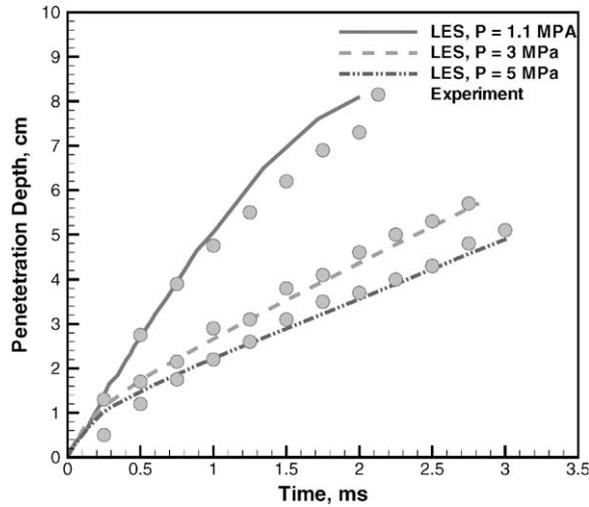
Fig. 3. Comparison of spray-tip penetration depth with experimental data at different chamber pressures.
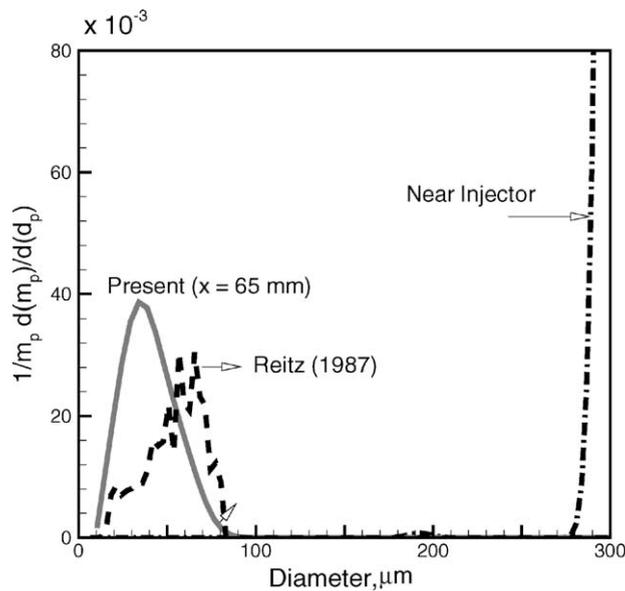

Fig. 4. Comparison of PDF of mass distribution for different droplet diameters with Reitz (1987) model, $P = 1.1$ MPa.

droplet diameter space near the injector and at $x = 65$ mm, respectively using the present sto-
chastic model and the wave model (Reitz, 1987). The evolution of the initial delta-function into a
broad-band distribution is clearly observed. It should be noted that the wave model does not
predict small size droplets at this location as compared to the stochastic model. The stripping of
small droplets is captured by the present model. In subsequent publications, a detailed compar-
ison of all the models using the present hybrid approach should be performed in order to evaluate
their performance.
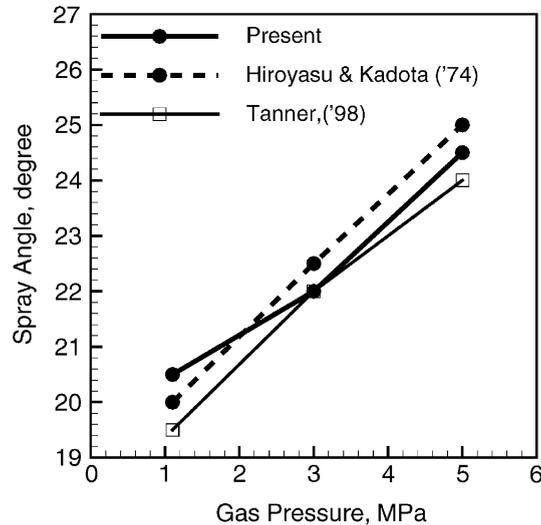
Fig. 5. Comparison of spray angles for different chamber pressures with the experimental data.

The spray angles produced for the three chamber pressures, 20°, 23°, and 25°, respectively, are in close agreement with the experimental observations as shown in Fig. 5. These angles are obtained for the present hybrid approach at the end of the simulation. The spray angle is determined by drawing a tangent to the radial spread of the spray starting from the end of the jet breakup. Computation of spray angle assures inclusion of 99% of the liquid mass in the whole domain. The agreement of the spray angle is also important to assess the accuracy of the breakup model, as it directly depends on the droplet-sizes produced and their momentum. Droplets with smaller size and thus smaller Stokes number have small relaxation time and follow the gas-phase flow. On the other hand, large droplets with higher inertia can move considerably farther against the surrounding gas-phase flow. Droplet size distributions predicted by the model should be such that the global spray angle is captured accurately.

Fig. 6 shows the evolution of the sauter mean diameter (SMD) for $P = 1.1$ MPa using the present model with hybrid approach and various other models usually used in commercial codes. Close to the injector, the SMD is around 300 μm corresponding to the size of the injected droplets. It decreases rapidly over a very short distance near the injector indicating atomization of parent blobs and remains more or less constant further downstream. At $x = 65$ cm, the experimental value from Hiroyasu and Kadota (1974) is also indicated. Only one point from the experiment is shown as the variation in SMD farther away from the nozzle is low. The under prediction of SMD away from the injector is expected because of lack of any coalescence model in the present simulation. Results from all other models shown make use of a coalescence model to obtain good agreement with the experimental data away from the injector. As seen from Fig. 6 different models predict different size distributions in the near-field and yet give the same results in the far-field. The SMD first decreases close to the injector and then increases when the coalescence dominates breakup. In the present simulations, we have purposefully neglected coalescence in order to indicate that the stochastic breakup model can predict the experimentally observed mist of small droplets stripped from the liquid core close to the injector. On the other hand, the present model
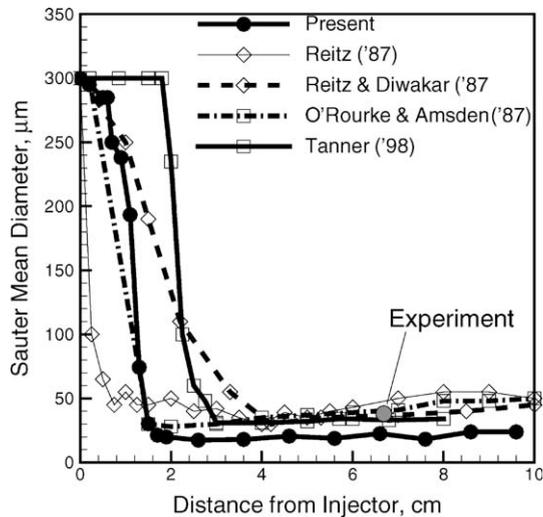
Fig. 6. Variation of sauter mean diameter (SMD) in the axial direction, $P = 1.1$ MPa.

does not predict excessive breakup as the liquid core lengths obtained from time evolution of the spray agree well with the experiments. A more detailed comparison of all the models with and without coalescence and using the present hybrid approach should be conducted to clearly identify the differences among them. This is not the scope of this work and will be conducted in the future.

Comparing the near-injector behavior of various models, Reitz and Diwakar (1987) show gradual decrease in SMD showing large size droplets beyond 2 cm. This model, however, does not show existence of small droplets close to the injector. Reitz (1987) improved this model to obtain small droplets close to the injector. These finely atomized drops decrease the spray surface area dramatically giving much smaller values of SMD. The TAB model by O'Rourke and Amsden (1987) also shows similar behavior near the injector. A liquid core of any significant length cannot be obtained by injecting large drops in the TAB model as these drops are highly unstable and burst into very small product droplets during first few computational time steps. The ETAB model by Tanner (1998) improves this by utilizing an exponential decay law to determine the product droplet sizes. This gives a significant core length as the SMD is more or less constant till 2 cm, however, does not show mist of stripped droplets close to the injector. In the present model, however, the size of newly formed droplets is obtained from a more general stochastic theory. This model thus shows SMD distributions near the nozzle in between that predicted by the TAB/wave and the ETAB models.

In order to assess the effectiveness of the hybrid-approach, the computations were performed using three different methods: tracking and creation of all droplets, tracking of parcels, and the hybrid droplet-parcel algorithm. Results are qualitatively compared to elucidate the differences among them. Fig. 7(a)–(c) shows the close-up views of spray near and further away from the nozzle at a certain time for the three different computational methods used, viz., pure droplets, pure parcels, and hybrid approach, respectively. The size of each circle plotted scales with the actual droplet diameters represented by the computational particle. Fig. 7(a) indicates presence
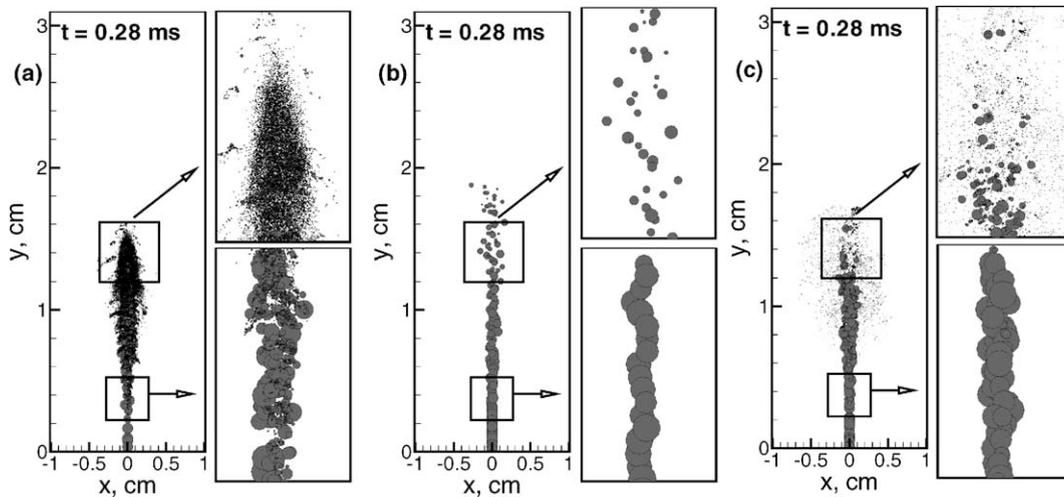
Fig. 7. Instantaneous snapshot of spray evolution using different computational approaches: (a) tracking all droplet trajectories, (b) parcels approach, (c) present hybrid approach. Size of the circles scales with the diameter of the droplets represented by the computational particle.

of a broad spectrum of droplet sizes with co-existence of large and small droplets as well as stripping breakup from the liquid core. This indicates the differences among the present stochastic breakup model and other the conventional deterministic models such as TAB (O'Rourke and Amsden, 1987) and Reitz (1987). It should be noted that, all droplet trajectories are computed giving large number of droplets ($\sim$500,000) even at an early stage of the simulation ($t = 0.28$ ms). This simulation, however, depicts the complex interactions between the liquid and gas-phases, the momentum coupling, and spray atomization due to stripping of small droplets.

Fig. 7(b) shows a similar simulation performed by using parcels-approach. An extremely coarse (global) representation of the liquid core and atomization is obtained because new droplets are not created. The total number of parcels injected into the domain at this stage is around 300. Fig. 7(c), on the other hand, indicates the effectiveness of the present hybrid approach. Here, the total number of computational particles ($\sim$6000) is much smaller than that shown in Fig. 7(a). Close to the nozzle, the liquid core shows existence of large and small droplets. Away from the nozzle, a global representation of droplets grouped to form parcels as well as small sparse droplets is observed. The computational overload due to the hybrid approach is significantly less ($\sim$50 times lower) in comparison with the computation of all droplet trajectories. On the other hand, the essential features of the spray dynamics are captured by the hybrid approach indicating its effectiveness and applicability in Eulerian–Lagrangian formulations.

Fig. 8 shows instantaneous spray field computed using the hybrid approach. Here the size of the circles scale with the total number of droplets represented by each computational particle. This clearly shows that, close to the injector each particle represents single blob injected (small circle size). After the liquid core length, the particles break and new computational particles are created. Based on the hybrid algorithm, these particles are grouped into bins and collected to form parcels (indicated by bigger size circles). The total number of trajectories computed can be easily limited
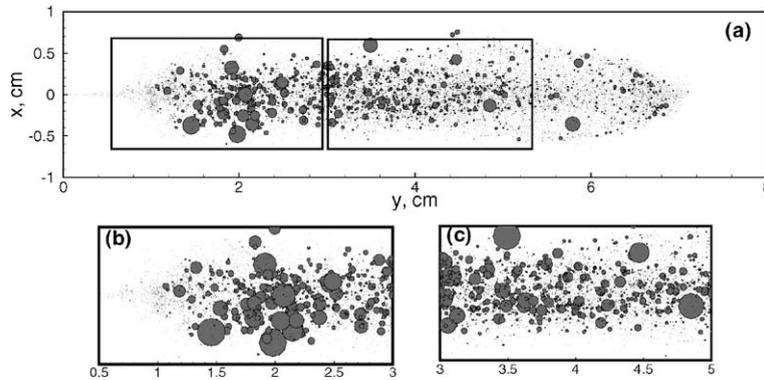
Fig. 8. Instantaneous snapshot of spray evolution using hybrid approach for $P = 1.1$ MPa. Size of the circles scales with the number of droplets represented by the computational particle: (a) full view, (b,c) close-up views.

by changing the threshold value of particles allowed in each computational cell and the total number of bins used to form the parcels.

6. Computation of air-blast atomization

Air-blast atomization of liquid jet in a strong, turbulent cross flow depicting conditions in a gas-turbine combustion chamber was also simulated using the hybrid-approach. First, a periodic, turbulent channel flow was computed using the unstructured LES code. The bulk mean velocity (U_c) normalized by the wall-shear velocity ($u_\tau = 1$ m/s) is approximately 15.63, which gives the Reynolds number based on the bulk mean velocity and full channel width as 5600. The gas-phase results for mean and r.m.s. values of the three velocity components show excellent agreement with the experiments as well as other DNS data and is reported by Mahesh et al. (2001). The coarse grid $32 \times 64 \times 32$ used in this simulation was able to give good results for the gas-phase turbulent quantities. Liquid jet is injected through the lower wall at $z = 0$ plane in the vertical direction with velocity 1/10th of the mean axial gas-phase velocity at the centerline of the channel (~18 m/s). The water jet is simulated by introducing 1 mm diameter blobs.

Fig. 9 shows the time evolution of gas-phase axial velocity contours in the $z = 0$ plane. Instantaneous snapshots of liquid spray are superimposed on the contour plots. The size of the circles is proportional to the droplet diameter. Axial velocity contours in a channel flow without liquid injection is also shown for comparison. It is seen that large-scale eddies transmit kinetic energy to the liquid jet, causing stretching, flapping, and breakup. A highly unsteady, 'pulsating' formation of droplets with broad size-spectrum is observed. The coupling between the gas-phase turbulent fluctuations and atomization is explored by computing one-point correlation between gas-phase streamwise velocity and droplet diameter as shown in Fig. 10. Strong correlation is observed in the core region of the liquid jet. The damping of turbulent fluctuations by the dense spray is evident from the contour plots shown in Fig. 9. This computation demonstrates the potential of the present stochastic breakup model along with the hybrid particle–parcel algorithm in simulating complex atomization process and spray dynamics. A systematic evaluation of these
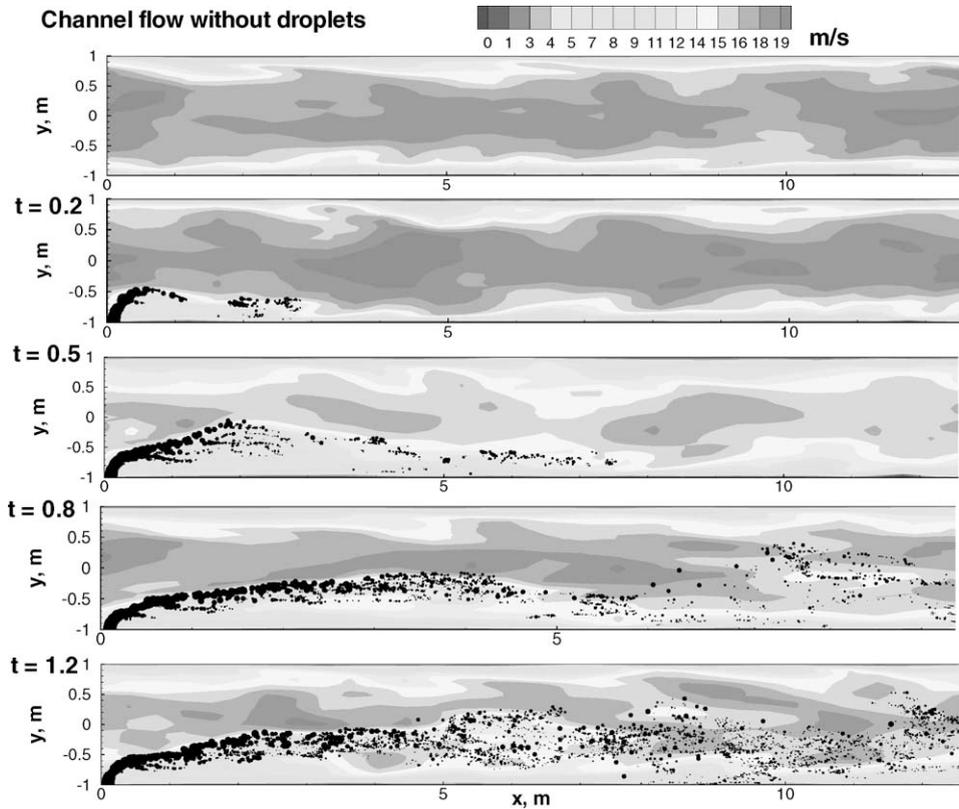
Fig. 9. Contours of axial velocity superimposed with instantaneous locations of the computational particles at $z = 0$. Droplets are injected from the bottom plane at $x = 0.01$ m.
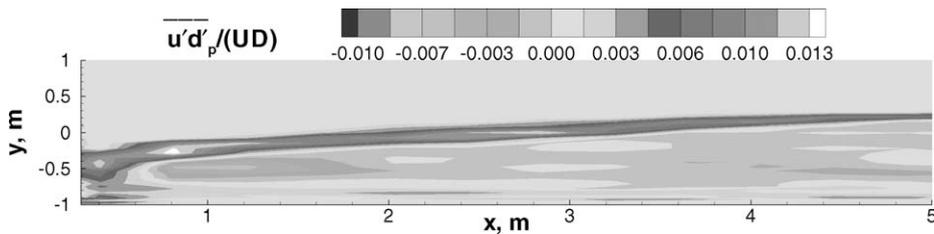

Fig. 10. One-point correlation between gas-phase velocity and droplet diameter normalized by reference velocity ($U = 1$ m/s) and channel width ($D = 2$ m).

modeling concepts in complex geometries can be done owing to considerable gain in computational time due to the hybrid approach.

7. Conclusion

A stochastic model for secondary breakup involving Lagrangian tracking of droplets with LES of the gas-phase flowfield was developed. Atomization was considered in the framework of cas-

cade of uncorrelated breakup events providing droplet diameter distribution with the critical stable diameter independent of the initial size. Kolmogorov's discrete model of particle breakup was represented by its Fokker–Planck approximation governing the production of new droplets. The parameters of the model were computed dynamically based on the local Weber number. The role of LES is to provide accurate predictions of turbulent transport used in estimating the maximum stable diameter of droplets before breakup. A novel hybrid-approach capable of simulating droplets as well as parcels was developed in the present work. This approach was shown to be highly efficient and more accurate compared to the standard parcels-approach usually employed in spray computations. The hybrid algorithm is particularly attractive in complex configurations with the presence of large number of droplets close to the injector. The present model was validated against available experimental data by Hiroyasu and Kadota (1974) and compared with other standard breakup models. A breakup simulation in the presence of turbulent cross flow was also performed to qualitatively demonstrate the effectiveness of the present model in air blast atomization.

Acknowledgements

References

Apte, S.V., Mahesh, K., Moin, P., 2003. Large eddy simulation of swirling, particle-laden flows. Int. J. Multiphase Flow 29, 1311–1331.

Chigier, N., Reitz, R.D., 1996. Regimes of jet breakup mechanisms (physical aspects). In: Kuo, K.K. (Ed.), In Recent Advances in Spray Combustion: Spray Atomization Drop Burning Phenomena, vol. 1, pp. 109–135.

Crowe, C., Sommerfeld, M., Tsuji, Y., 1998. Multiphase Flows with Droplets and Particles. CRC Press, Boca Raton, FL.

Dukowicz, J.K., 1980. A particle-fluid numerical model for liquid sprays. J. Comput. Phys. 35, 229.

Faeth, G.M., Hsiang, L.P., Wu, P.K., 1995. Structure and breakup properties of sprays. Int. J. Multiphase Flow 21, 99–127.

Gel'fand, B.E., Gubin, S.A., Kogarko, S.M., Komar, S.P., 1975. Singularities of the breakup of viscous liquid droplets in shock waves. J. Eng. Phys. 25, 1140–1142.

Georjion, T.L., Reitz, R.D., 1999. A drop-shattering collision model for multidimensional spray computations. Atomization Sprays 9, 231–254.

Gorokhovski, M.A., 2001. The stochastic lagrangian model of drops breakup in the computation of liquid sprays. Atomization Sprays 11, 505–520.

Gorokhovski, M.A., Saveliev, V.L., 2003. Analyses of Kolmogorov's model of breakup and its application into Lagrangian computation of liquid sprays under air-blast atomization. Phys. Fluids 15, 184–192.

Hiroyasu, M., Kadota, T., 1974. Fuel droplet size distribution in diesel combustion chamber, SAE Paper 74071.

Kolmogorov, A.N., 1941. On the log-normal distribution of particles sizes during breakup process. Dokl. Akad. Nauk. SSSR XXXI (2), 99–101.

Kolmogorov, A.N., 1949. On the drop breakup in turbulent flows. Gidromekanika, DAN LXVI (NS), 825–828.

Kuznezov, V.R., Sabel'nikov, V.A., 1990. Turbulence and Combustion. Hemisphere, New York.

Lefebvre, A.H., 1989. Atomization & Sprays. Hemisphere, New York.

Mahesh, K., Constantinescu, G., Apte, S., Iaccarino, G., Moin, P., 2001. Large-eddy simulation of gas turbine combustors. Annual Research Briefs, Center for Turbulence Research, NASA Ames/Stanford University.

Mahesh, K., Constantinescu, G., Moin, P., 2003. A new time-accurate finite-volume fractional-step algorithm for prediction of turbulent flows on unstructured hybrid meshes. J. Comput. Phys., submitted.

Martinez-Bazan, C., Montanes, J.L., Lasheras, J.C., 1999. On the breakup of an air bubble injected into a fully developed turbulent flow. Part 1. Breakup frequency. J. Fluid Mech. 401, 157–182.

Moin, P., Kim, J., 1987. Numerical investigation of turbulent channel flow. J. Fluid Mech. 118, 341–377.

O'Rourke, P.J., 1981. Collective drop effects on vaporizing liquid sprays. Ph.D. Thesis 1532-T, Princeton University.

O'Rourke, P.J., Amsden, A.A., 1987. The TAB method for numerical calculations of spray droplet breakup. SAE Technical Paper 87-2089.

Pilch, M., Erdman, C.A., 1987. Use of breakup time data and velocity history data to predict the maximum size of stable fragments for acceleration-induced breakup of a liquid drop. Int. J. Multiphase Flow 13, 741–757.

Reitz, R.D., 1987. Modeling atomization processes in high-pressure vaporizing sprays. Atomization Spray Tech. 3, 307.

Reitz, R.D., Diwakar, R., 1987. Structure of high presure fuel sprays. SAE Technical Paper 870598.

Schmidt, D.P., Rutland, C.J., 2000. A new droplet collision algorithm. J. Comput. Phys. 164, 62–80.

Shavit, U., Chigier, N., 1995. Fractal dimensions of liquid jet interface under breakup. J. Atomization Sprays 5, 525–543.

Tanner, F.X., 1998. Liquid jet atomization and droplet breakup modeling of non-evaporating diesel fuel sprays. SAE Transactions: J. Engines 106, 127–140.

Zhou, W.X., Yu, Z.H., 2000. Multi-fractality of drop breakup in the air-blast nozzle atomization process. Phys. Rev. E 63, 016302.